LA-UR-22-22586

Approved for public release; distribution is unlimited.

Title:	Surface Roughness Calculations of Additively Manufactured Cylinders via X-Ray Computed Tomography
Author(s):	Hunter, Bryan Keeney
Intended for:	Report
Issued:	2022-03-18

Surface Roughness Calculations of Additively Manufactured Cylinders via X-Ray Computed Tomography

Bryan K. Hunter[1,*]

[1]Engineered Materials Group, Materials Science and Technology Division, Los Alamos National Laboratory, Los Alamos, NM 87545, USA.

KEYWORDS: X-ray computed tomography, additive manufacturing, powder bed fusion, and surface roughness

ABSTRACT: X-ray Computed Tomography (X-ray CT) is an analytical technique used in materials science to non–destructively characterize features in variety of materials like polymers, metals, composites, and explosives. It also has the capability of imaging additively manufactured, machined and assembled parts and processes. The non-destructive imaging allows for the analysis of features (voids and cracks), which give a fundamental understanding of material characteristics. Additionally, X-ray CT can obtain accurate measurements of dimensional and topographic variations as a result of different stimuli, and assess accuracy of material production. This study will focus on parts manufactured via metal additive manufacturing (AM). Although, AM produces parts faster and easier, the printing process can produce defects (pores and surface roughness) that undermine the part's mechanical properties. The analysis of 3D printed objects has a strength in analysis in that the material has an STL file from which the item was printed, which is not available in many manufactured materials (i.e. foams) due to stochastic structures. For this study, the print accuracy of several 3D printed cylinders will be assessed via X-ray CT to determine optimal printing parameters for parts with less defects and stronger mechanical properties. This will be accomplished by having the original STL file serve as the baseline surface to compute difference in the CT rendering to calculate surface roughness for each cylinders.

Introduction

X-ray computed tomography (X-ray CT) is analytical technique used in material science for the non-destructive characterization of an array of different materials like polymers, metals, composites and explosives. X-ray CT has the capability of imaging defects such as cracks, voids, pores and other defects to understand and answer questions about material characteristics [1–3]. In addition to detecting defects, X-ray CT can be used to obtain accurate measurements on dimensional and topographic variations due to different stimuli, and to assess the accuracy and quality of material production.

X-ray CT is also popular for the imaging of machined, assembled and additively manufactured parts. This study focuses on additively manufactured parts as the method has grown in popularity. This is due to additive manufacturing (AM) being a more versatile method that can produce lighter, stronger parts faster. AM is an umbrella term referring to a multitude of different AM technologies such as material extrusion, vat photopolymerization, and metal laser powder bed fusion (L-PBF)[4]. The L-PBF processes is the most popular and extensively researched techniques for metal printing due to its low cost, recyclability of powder, materials available to print with, and lack of a need for a minimum support during the printing process [5–8]. However, it does have some issues as defects (e.g., surface roughness) can arise during printing. The development of these defects depend on several factors like the build direction, the powder being used or the number of parts present on the build plate [9,10]. These defects impact the mechanical properties of the part, and make it more likely to fail.[11] Therefore, it is important to determine the optimal build parameters to minimize these defects and strengthen the parts mechanical properties. X-ray CT is commonly used to analyze these defects post-printing as a ground truth understanding of material characteristics. Additionally, X-ray CT can be used to assess the accuracy and quality for both the exterior and interior surfaces of a print, which is important in assessing the successfulness of an AM technique.

The current literature on assessing defects in AM parts tends to focus on defects like porosity or cracks to assess print accuracy [12,13]. This study, however, is interested in looking at the surface roughness because it can gives a more accurate analysis of print accuracy. Surface roughness in the current literature is often mentioned briefly and only as supplementary information as the focus is often on analyzing other defect or stating the general capabilities of X-ray CT [14–17]. That being said, surface roughness has been previously used as a method for determining print accuracy. In these studies, X-ray CT is used to obtain a 2D slice of the surface and the surface roughness is calculated via the derivations from the baseline surface [18–20]. This method is similar to what has traditionally been used in profilometric techniques. While this method does give information about the surface roughness, it only gives information for a small area on the surface. All areas of the surface are important to consider when assessing the print accuracy for an additively manufactured part. More surface inclusive techniques are being explored that overlay the reconstructed CT rendering onto the original STL design[21–23]. In this case, the STL

serves as the baseline surface from which the differences in the CT rendering are quantified to calculate surface roughness. This technique can give a more accurate value for surface distance and better assess the print quality as both the inner and outer surfaces are considered in the calculations.

This study aims to use X-ray CT to determine the print accuracy of several additively manufactured metal cylinders by using the original STL file as a baseline surface from which differences in the X-ray CT data can be measured. By determining surface roughness in this manner, the print accuracy can be understood and quantified. By comparing the print accuracy for several cylinders printed with variable scanning speeds, laser power, and focus diameter, the optimal printing parameters can be determined to produce additively manufactured parts with less defects and stronger mechanical properties.

Experimental Methods

Column Design

The cylinders were designed using Solidworks (Dassault Systèmes SE, LLC) CAD software and were designed with a grooved pattern on the edges to assess printing accuracy for more complex geometries (Figure 1)

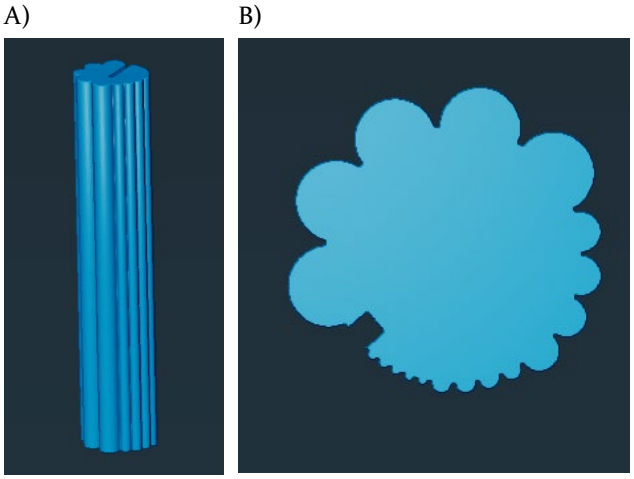

Figure 1. Example CAD cylinder design: A) side view of grooves and B) Top view of groove pattern.

Column 3D Printing

The columns were printed on an EOS (Krailling, Germany) M90 3D-printer using 319L stainless steel as the base powder. The instrument utilizes a 400 W ytterbium-fiber laser with F-theta lens and high speed scanner. It has scanning speed up to 7.0 m/s (23 ft/s) and a focus diameter of 100 µm. Each cylinder was printed at different scanning speeds, laser power, and focus diameter to determine the optimal printing parameters. Cylinder 1 was printed with a laser power of 200 W and a focus diameter of 78 µm. Cylinder 4 was printed with a laser power of 220 W and a focus diameter of 60 µm. Cylinder 7 was printed with a laser power of 220 W and a laser diameter of 78 µm.

Tomographic Imaging

The X-ray CT images were collected using a Carl Zeiss X-ray Microscopy Inc. (Dublin, CA) Xradia Versa 520 microXCT. The instrument has a tungsten transmission anode X-ray source in a cone-beam geometry. Sample imaging conditions included an applied voltage of 110 kVp, an applied current of 91 µA, 10 W power, a camera binning of 1, HE 18 source filter, flat panel detector, and 14 s exposure time per radiograph. Each sample was rotated 360° per tomogram to collect 4501 radiographs with a pixel size of 4.8251 µm. Each scan took about 18 hours to complete. After scan completion, reconstruction was performed in Xradia XMReconstructor software.

Image Processing

All cylinders were rendered in 3D using Avizo 2021.2 software (Thermo Fischer Scientific, Waltham, MA). The X-ray CT images were cropped and edited with "fill holes" and "remove small spots" functions. The STL file was also cropped and transformed to the same dimensions as the X-ray CT 3D rendering. The STL file and CT rendering were aligned in Avizo, so that the two surface were overlaid as closely as possible. This alignment is important for accurately calculating the surface distances. Additionally, the end surfaces were removed to improve the measurements by removing artificial surfaces. These artificial surfaces can skew the measurements, so they do not accurately model surface roughness

After the STL file and X-ray CT renderings were aligned and the end surfaces were removed, the distance between the two surfaces were calculated. The deviations from the baseline surfaces were visualized using the physicsNDT color map.

Surface Roughness Calculations

The surface roughness was calculated using several different definitions for surface roughness. R_a signifies the roughness average of the entire surface, and it is represented by the equation below:

$$R_a = \frac{1}{MN}\sum_{j=1}^{M}\sum_{i=1}^{N}|Z_{ji}|$$

This equation represents the arithmetic mean of the absolute values for the surface departures from the mean plane. R_q signifies the root mean square (RMS) roughness, and is represented by the equation:

$$R_q = \sqrt{\frac{1}{MN}\sum_{j=1}^{M}\sum_{i=1}^{N} Z^2(x_i, y_j)}$$

The R_p value signifies the maximum profile peak height, which is the distance between the highest point on the surface and the zero surface. Similarly, R_v signifies the maximum profile valley depth, which represents the distance between the lowest point on the surface and the zero surface. R_t signifies the maximum height of the surface, which is the vertical distance between the highest and lowest points on the surface. It is represented by the equation:

$$R_t = R_p + R_v$$

Results and Discussion

A)

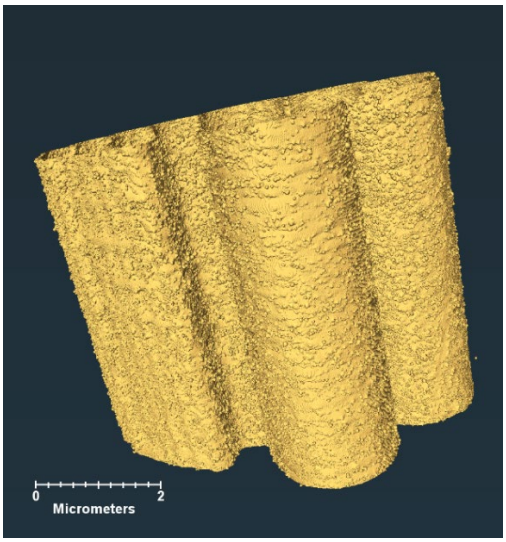

B)

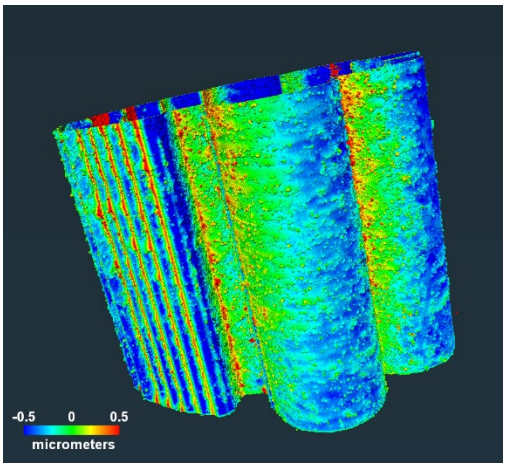

Figure 2. CT rendering examples: A) CT surface rendering of cylinder 4 and B) CT rendering of cylinder 4 with PhysicsNDT colormap applied to show surface roughness. Green represents the baseline surface, red represents positive deviations from the baseline, and blue represents negative deviations from the baseline surface.

A set of three cylinders were analyzed via X-ray CT, and this data was overlaid onto the original STL files for each cylinder (Figure 2A). The STL file served as the base surface, and any difference from that surface in the CT rendering represented the surface roughness for each cylinder. As shown in Figure 2B, all cylinders show some variations in distance from the zero surface with the grooved regions showing dimensional variations. This shows the limitations of 3D printing when it comes to sharp features like the grooves in these cylinders. The dimensional accuracy as a result of the printing process was low and the printed samples did not produce an accurate groove. Additionally, the larger curved regions of each cylinder show far less surface roughness on the outer surface then is observed in the smaller curved regions. These areas are where the highest amount of surface roughness is concentrated in each of the cylinders. This shows that in addition to sharp features metal 3D printing has difficulties with producing small finer features. Both of these limitations are important considerations for the dimensional accuracy and part performance as the surface roughness can affect the mechanical properties of the part[24]. These limitations also restrict the minimum feature size available to print as features smaller or equal to the surface roughness will not be achievable with a high level of accuracy.

	R_a (mm)	R_q (mm)	R_p (mm)	R_v (mm)	R_t (mm)
Cylinder 1	0.0337 ± 0.06	0.0733 ±0.1	1.14	-0.769	0.370
Cylinder 4	0.0379 ±0.05	0.0541 ±0.1	0.873	-0.370	0.503
Cylinder 7	0.0444 ±0.06	0.0765 ±0.1	0.943	-0.213	0.730

Table 1. Surface roughness values for cylinders 1, 4 and 7

Cylinder 1 seems to have the lowest R_a value, which is usually the most reliable for determining surface roughness variations However, the standard deviations for all three cylinder's R_a value are all larger than the calculated value. This suggests that there is a wide numerical spread from the reported mean values in Table 1. Therefore, it was concluded that all three cylinders had statistically the same values for both the R_a and R_v, meaning that they all had the same levels of surface roughness. This conclusion from these calculations is supported by the high surface roughness visualized in the CT renderings

like in Figure 2. All three cylinders showed similar amount of surface roughness in roughly all the same regions (grooves and fine features). This prevented any conclusions from being made about the effectiveness to decrease the surface roughness between cylinder's printing parameters. This is also an important result as cylinder 1 used the standard printing parameters also used for more complex parts. According to these results, there is no negligible difference when those difference are changed. Therefore, it will be important in future studies to optimize printing parameters further to minimize surface roughness, so that a noticeable decrease can be observed via the proposed method.

Conclusion

X-ray CT is a versatile method used in materials science for the analysis of a variety of different materials and manufacturing processes. It is often used to identify defect or dimensional and topographic changes in metal AM parts to assess print accuracy and material characteristics. This study focused on surface roughness, which is not as widely studied as other defects like porosity or cracks. However, it arguably gives the clearest understanding of print accuracy and material characteristics. Three cylinders all printed with different printing parameters were analyzed in order to determine the optimal parameters to produce materials with the least surface roughness. The surface roughness was quantified using a method of overlaying the original STL file and the CT rendering. The STL serves as the baseline surface and the deviations from that surface in the CT rendering are used to calculate surface roughness. It was concluded that all three cylinders had statistically the same surface roughness values, and as a result comparable levels of surface roughness. This conclusion prevented any conclusions from being made about each cylinder's printing parameters being deemed the most optimal for decreasing surface roughness. Additionally, this suggests that the printing parameters can be further investigated to minimize defects and to improve print accuracy. Future work hopes to expand upon this work and further optimize the printing parameters by analyzing more cylinders to achieve parts with fewer dimensional variations and lower surface roughness.

AUTHOR INFORMATION

Corresponding Author

*Bryan K. Hunter – bkhunter@lanl.gov, Engineered Materials Group, Materials Science and Technology Division, Los Alamos National Laboratory, Los Alamos, NM, 87545, USA.

ACKNOWLEDGMENT

Funding for this research was provided by Adam Wachtor of the LANL Engineering Institute under LDRD-ER project 20220368ER

ABBREVIATIONS

X-ray CT, X-ray Computed Tomography; AM, Additive Manufacturing; L-PBR, Laser Powder Bed Fusion.

REFERENCES

(1) Patterson, B. M.; Kuettner, L.; Shear, T.; Henderson, K.; Herman, M. J.; Ionita, A.; Chawla, N.; Williams, J.; Sun, T.; Fezzaa, K.; Xiao, X.; Welch, C. Synchrotron CT Imaging of Lattice Structures with Engineered Defects. *J Mater Sci* **2020**, 55 (25), 11353–11366. https://doi.org/10.1007/s10853-020-04840-y.

(2) Stock, S. R. X-Ray Microtomography of Materials. *International Materials Reviews* **1999**, *44* (4), 141–164. https://doi.org/10.1179/095066099101528261.

(3) Withers, P. J.; Bouman, C.; Carmignato, S.; Cnudde, V.; Grimaldi, D.; Hagen, C. K.; Maire, E.; Manley, M.; Du Plessis, A.; Stock, S. R. X-Ray Computed Tomography. *Nat Rev Methods Primers* **2021**, *1* (1), 18. https://doi.org/10.1038/s43586-021-00015-4.

(4) Calignano, F.; Manfredi, D.; Ambrosio, E. P.; Biamino, S.; Lombardi, M.; Atzeni, E.; Salmi, A.; Minetola, P.; Iuliano, L.; Fino, P. Overview on Additive Manufacturing Technologies. *Proceedings of the IEEE* **2017**, *105* (4), 593–612. https://doi.org/10.1109/JPROC.2016.2625098.

(5) Singh, R.; Gupta, A.; Tripathi, O.; Srivastava, S.; Singh, B.; Awasthi, A.; Rajput, S. K.; Sonia, P.; Saxena, K. Powder Bed Fusion Process in Additive Manufacturing: An Overview | Elsevier Enhanced Reader. *Materials Today: Proceedings* **2020**, *26*, 3058–3070. https://doi.org/10.1016/j.matpr.2020.02.635.

(6) Priarone, P. C.; Lunetto, V.; Atzeni, E.; Salmi, A. Laser Powder Bed Fusion (L-PBF) Additive Manufacturing: On the Correlation between Design Choices and Process Sustainability. *Procedia CIRP* **2018**, *78*, 85–90. https://doi.org/10.1016/j.procir.2018.09.058.

(7) Vock, S.; Klöden, B.; Kirchner, A.; Weißgärber, T.; Kieback, B. Powders for Powder Bed Fusion: A Review. *Prog Addit Manuf* **2019**, *4* (4), 383–397. https://doi.org/10.1007/s40964-019-00078-6.

(8) Gorji, N. E.; Saxena, P.; Corfield, M.; Clare, A.; Rueff, J.-P.; Bogan, J.; Gonzalez, P. G. M.; Snelgrove, M.; Hughes, G.; O'Connor, R.; Raghavendra, R.; Brabazon, D. A New Method for Assessing the Recyclability of Powders within Powder Bed Fusion Process. *Material Characterization* **2020**, *161*, 110167. https://doi.org/10.1016/j.matchar.2020.110167.

(9) Martin, A. A.; Calta, N. P.; Khairallah, S. A.; Wang, J.; Depond, P. J.; Fong, A. Y.; Thampy, V.; Guss, G. M.; Kiss, A. M.; Stone, K. H.; Tassone, C. J.; Nelson Weker, J.; Toney, M. F.; van Buuren, T.; Matthews, M. J. Dynamics of Pore Formation during Laser Powder Bed Fusion Additive Manufacturing. *Nat Commun* **2019**, *10* (1), 1987. https://doi.org/10.1038/s41467-019-10009-2.

(10) Khairallah, S.; Anderson, A. T.; Rubenchick, A.; King, W. E. Laser Powder-Bed Fusion Additive Manufacturing: Physics of Complex Melt Flow and Formation Mechanisms of Pores, Spatter, and Denudation Zones | Elsevier Enhanced Reader. *Acta Materialia* **2016**, *108*, 36–34. http://dx.doi.org/10.1016/j.actamat.2016.02.014.

(11) du Plessis, A.; Yadroitsava, I.; Yadroitsev, I. Effects of Defects on Mechanical Properties in Metal Additive Manufacturing: A Review Focusing on X-Ray Tomography Insights | Elsevier Enhanced Reader. *Materials and Design* **2020**, *187*, 108385. https://doi.org/10.1016/j.matdes.2019.108385.

(12) Thompson, A.; Maskery, I.; Leach, R. K. X-Ray Computed Tomography for Additive Manufacturing: A Review. *Meas. Sci. Technol.* **2016**, *27* (7), 072001. https://doi.org/10.1088/0957-0233/27/7/072001.

(13) Du Plessis, A. Effects of Process Parameters on Porosity in Laser Powder Bed Fusion Revealed by X-Ray Tomography. *Additive Manufacturing* **2019**, *30*, 100871. https://doi.org/10.1016/j.addma.2019.100871.

(14) Khosravani, M. R.; Reinicke, T. On the Use of X-Ray Computed Tomography in Assessment of 3D-Printed Components. *J Nondestruct Eval* **2020**, *39* (4), 75. https://doi.org/10.1007/s10921-020-00721-1.

(15) Towsend, A.; Senin, N.; Blunt, L.; Leach, R. K.; Taylor, J. S. Surface Texture Metrology for Metal Additive Manufacturing: A Review | Elsevier Enhanced Reader. *Precision Engineering* **2016**, *46*, 34–47. http://dx.doi.org/10.1016/j.precisioneng.2016.06.001.

(16) Zanini, F.; Sbettega, E.; Carmignato, S. X-Ray Computed Tomography for Metal Additive Manufacturing: Challenges and Solutions for Accuracy Enhancement. *Procedia CIRP* **2018**, *75*, 114–118. https://doi.org/10.1016/j.procir.2018.04.050.

(17) du Plessis, A.; Yadroitsev, I.; Yadroitsava, I.; Le Roux, S. G. X-Ray Microcomputed Tomography in Additive Manufacturing: A Review of the Current Technology and Applications. *3D Printing and Additive Manufacturing* **2018**, *5* (3), 227–247. https://doi.org/10.1089/3dp.2018.0060.

(18) Lifton, J. J.; Liu, Y.; Tan, Z. J.; Mutiargo, B.; Goh, X. Q.; Malcolm, A. A. Internal Surface Roughness Measurement of Metal Additively Manufactured Samples via X-Ray CT: The Influence of Surrounding Material Thickness. *Surf. Topogr.: Metrol. Prop.* **2021**, *9* (3), 035008. https://doi.org/10.1088/2051-672X/ac0e7c.

(19) Klingaa, C. G.; Dahmen, T.; Baier, S.; Mohanty, S.; Hattel, J. H. X-Ray CT and Image Analysis Methodology for Local Roughness Characterization in Cooling Channels Made by Metal Additive Manufacturing. *Additive Manufacturing* **2020**, *32*, 101032. https://doi.org/10.1016/j.addma.2019.101032.

(20) Thompson, A.; Senin, N.; Giusca, C.; Leach, R. Topography of Selectively Laser Melted Surfaces: A Comparison of Different Measurement Methods. *CIRP Annals* **2017**, *66* (1), 543–546. https://doi.org/10.1016/j.cirp.2017.04.075.

(21) Kerckhofs, G.; Pyka, G.; Moesen, M.; Van Bael, S.; Schrooten, J.; Wevers, M. High-Resolution Microfocus X-Ray Computed Tomography for 3D Surface Roughness Measurements of Additive Manufactured Porous Materials. *Advanced Engineering Materials* **2013**, *15* (3), 153–158. https://doi.org/10.1002/adem.201200156.

(22) Fritsch, T.; Farahbod-Sternahl, L.; Serrano-Muñoz, I.; Léonard, F.; Haberland, C.; Bruno, G. 3D Computed Tomography Quantifies the Dependence of Bulk Porosity, Surface Roughness, and Re-Entrant Features on Build Angle in Additively Manufactured IN625 Lattice Struts. *Adv Eng Mater* **2021**, 2100689. https://doi.org/10.1002/adem.202100689.

(23) Karme, A.; Kallonen, A.; Matilainen, V.-P.; Piili, H.; Salminen, A. Possibilities of CT Scanning as Analysis Method in Laser Additive Manufacturing. *Physics Procedia* **2015**, *78*, 347–356. https://doi.org/10.1016/j.phpro.2015.11.049.

(24) Yanez, A.; Fiorucci, M. P.; Cuadrado, A.; Martel, O.; Monopoli, D. Surface Roughness Effects on the Fatigue Behaviour of Gyroid Cellular Structures Obtained by Additive Manufacturing. *International Journal of Fatigue* **2020**, *138*, 105702. https://doi.org/10.1016/j.ijfatigue.2020.105702.